

# Rabi Spectroscopy and Sensitivity of a Floquet Engineered Optical Lattice Clock

Mo-Juan Yin,<sup>1,\*</sup> Tao Wang,<sup>2,\*</sup> Xiao-Tong Lu,<sup>1</sup> Ting Li,<sup>1</sup> Ye-Bing Wang,<sup>1</sup>  
Xue-Feng Zhang,<sup>2,†</sup> Wei-Dong Li,<sup>3,‡</sup> Augusto Smerzi,<sup>3,4,§</sup> and Hong Chang<sup>1,5,¶</sup>

<sup>1</sup>Key Laboratory of Time and Frequency Primary Standards,  
National Time Service Center, Chinese Academy of Sciences, Xi'an 710600, China

<sup>2</sup>Department of Physics, and Center of Quantum Materials and Devices,  
Chongqing University, Chongqing, 401331, China

<sup>3</sup>Department of Physics and Institute of Theoretical Physics, Shanxi University, Taiyuan 030006, China

<sup>4</sup>QSTAR, INO-CNR, and LENS, Largo Enrico Fermi 2, I-50125 Firenze, Italy

<sup>5</sup>School of Astronomy and Space Science, University of Chinese Academy of Sciences, Beijing 100049, China

Floquet engineering is a powerful tool to customize quantum states and Hamiltonians via time-periodic fields. In this manuscript, we periodically modulate the lattice potential of a  $^{87}\text{Sr}$  optical clock. Different from previous works where the external (spatial) single-particle energies are manipulated, we target the internal (atomic) degrees of freedom and engineer the optical clock transition. We shape Floquet quasi-energies and measure their resonance profiles with Rabi spectroscopy. We provide the spectroscopic sensitivity of each band by measuring the Fisher information and show that this is not depleted by the Floquet dynamical modulation. The demonstration that the internal degrees of freedom can be selectively engineered by manipulating the external degrees of freedom inaugurates a novel device for metrology, sensing and quantum technologies.

*Introduction.* — The coherent manipulation of quantum systems using periodic modulations, also known as Floquet engineering (FE), is becoming a central paradigm for the realization of synthetic quantum states and Hamiltonians [1–3]. FE has been demonstrated in a variety of different platforms including ultra-cold atoms [1], photonics [4] and superconducting qubits systems [5]. In the context of atomic gases trapped in driven optical lattices [1], the periodic modulation has been employed to renormalize the parameters of the Hubbard Hamiltonian. In particular, the dynamical modulation can be recast into an effective tunable tunneling. This has led to the demonstration of coherent destruction of tunneling [6], dynamical control of superfluid-insulator phase transitions [7], artificial gauge fields [8–10] and topological lattice models [11–14].

On the other hand, the optical lattice clock (OLC) is among the most accurate precision measurement devices [15–18]. It sets the ground for next standard of time and several proposals aim to exploit their extraordinary stability and accuracy to address fundamental problems ranging from the measurements of physical constants [19] to the detection of gravitational waves [20],[21]. OLC consists of an optical local oscillator stabilized by an appropriately chosen two energy levels transition of several atoms trapped in a stationary lattice potential [22]. Usually, a lattice field can significantly modify the transition energies. In OLC, this problem is addressed by engineering the magic-wavelength transition of  $^{87}\text{Sr}$  atoms that is well known to be insensitive to the external trap thanks to a first-order light shift cancellation [17]. Considering the spontaneous emission of the  $^{87}\text{Sr}$  excited clock state becomes important in about 160 s, the OLC becomes an ideal candidate for Floquet engineering the internal (atomic) energy distribution.

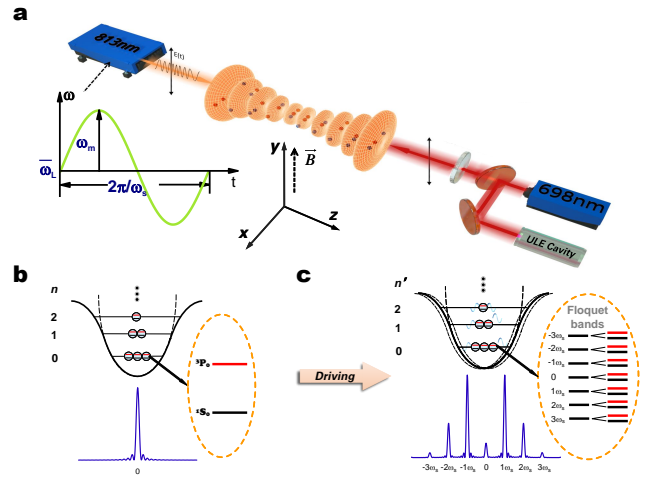


Figure 1. (a) The optical lattice potential is made by a counter-propagating laser ( $\lambda_L = 813$  nm) along the  $z$  direction. The beam waist ( $W_0 = 50$   $\mu\text{m}$ ) locates the center of the magneto-optical trap (MOT) and its distance from the high-reflecting mirror is  $L \simeq 0.3$  m. The clock laser ( $\lambda_p = 698$  nm) is locked to the ultralow-expansion (ULE) glass cavity and nearly aligned along the same direction of the lattice laser to excite the clock transition. The Floquet modulation (FM) of the lattice laser is controlled with a build-in piezo actuator. (b) At magic-wavelength  $\lambda_L$  only one sharp peak at the clock transition is observed in the Rabi spectroscopy (blue curve). (c) When turning on the periodic driving, the carrier peak is split into several Floquet bands as observed in the Rabi spectroscopy (blue curve) and schematically shown in the oval inset.

In this manuscript, we demonstrate Floquet clock bands realized with a dynamical periodic modulation of the trapping potential. We show that the atomic spin population dynamics is governed by a periodi-

cally driven Landau-Zener-Stuckelberg-Majorana Hamiltonian (LZSM) [23, 24]. We resolve several Floquet quasi-energy bands with ultra-sensitive Rabi spectroscopy. Each band consists on the optical clock transition modified by multiples of the driving frequency. The number and the shape of the resonance peaks are controlled by an opportunely tailored multi-frequency driving. We study the spectroscopic sensitivity of each band by measuring the Fisher information, which provides the ultimate bound in sensitivity in parameter estimation theory [25, 26]. We show the sensitivity is unaffected by the Floquet shaking potential demonstrating that, on the time scales of our experiments, dynamically induced decoherences and thermalization effects can be ignored. Our work opens to the design of a new generation of devices for sensing, metrology and quantum simulations where the internal energy structure of an optical lattice clock can be engineered by manipulating the motional atomic degrees of freedom.

*Experiment set-up.* — Approximately  $10^4$  fermionic  $^{87}\text{Sr}$  atoms are cooled down to  $3\mu\text{K}$  and loaded in a quasi one-dimensional optical lattice aligned with the  $z$  axis. The lattice is created by a counter-propagating laser beam at magic-wavelength  $\lambda_L = 813\text{ nm}$  [27, 28] (Fig. 1a), so that the atoms at the dipole-forbidden transition energy levels  $(5s^2)^1\text{S}_0(|g\rangle)$  and  $(5s5p)^3\text{P}_0(|e\rangle)$  feel the same lattice potential [17] (Fig. 1b). We load about one thousand lattice sites separated by barriers of height  $V_0/E_r \approx 90$  ( $E_r$  is the recoil energy) which hinder inter-site tunneling. We Floquet engineer our system by periodically driving the piezo actuator. The frequency of the lattice laser is modulated as  $\omega_L(t) = \bar{\omega}_L + f(t)$ , where  $\bar{\omega}_L = 2\pi c/\lambda_L$  is the average lattice carrier frequency and

$$f(t) = \sum_{m=1}^N \omega_m \sin(\omega_s m t) \quad (1)$$

is a  $T = 2\pi/\omega_s$  periodic  $N$ -modes function.

In the following we first consider a monochromatic driving  $f(t) = \omega_1 \sin(\omega_s t)$ , while a multi-mode driving will be discussed later. The intensity of the lattice laser along the  $z$  direction becomes  $I = I_0 \sin^2(\bar{\omega}_L(z + \int v(t)dt)/c)$ , where  $v(t) \simeq \omega_1 \omega_s L \cos(\omega_s t)/\bar{\omega}_L$  is an effective lattice velocity. In the lattice co-moving frame, the frequency of the optical clock laser (CL)  $\omega_p$  is shift to  $\omega'_p(t) = (1 - v(t)/c)\omega_p$  due to the relativistic Doppler effect.

*Model.* — The Hamiltonian of a single atom interrogated by the clock laser and trapped in a driven periodic potential can be written as  $\hat{H} = \hat{H}_{\text{ext}} + \hat{H}_{\text{int}} + \hat{H}_c$ , where

$$\begin{aligned} \hat{H}_{\text{ext}} = & \left[ \frac{\hat{p}^2}{2M} + \frac{\alpha_0 I_0}{2\epsilon_0 c} e^{-2r^2/w_0^2} \sin^2\left(\frac{\bar{\omega}_L}{c} z\right) \right. \\ & \left. - \frac{M\omega_m \omega_s^2 L}{\bar{\omega}_L} z \sin(\omega_s t) \right] \hat{\sigma}^{(0)}, \end{aligned} \quad (2)$$

governs the motion of the center of mass of the atom and

$$\hat{H}_c = \frac{\alpha_c I_0}{4\epsilon_0 c} \sin(\omega_s t) \sin^2\left(\frac{\bar{\omega}_L}{c} z\right) \hat{\sigma}^{(3)} \quad (3)$$

is coupling Hamiltonian provided by a spin-dependent optical lattice potential (notice that this term has a purely dynamical origin, while spin-dependent periodic potentials have been previously created with polarized standing waves laser fields [29, 30]). The parameter  $\alpha_c$  is proportional to the difference between the polarizability derivatives of the two spin states calculated at the magic-wavelength. We have chosen the values of the coupling constant  $\frac{\alpha_c I_0}{4\epsilon_0 c} \approx 1\text{Hz}$  so that Eq.3 can be neglected on times scales of the order of a second. This is of the same order of the dephasing time of our optical lattice clock caused by the finite temperature of the atomic sample. The spin dynamics of the atomic gas is governed by the Landau-Zener-Stuckelberg-Majorana Hamiltonian [24]:

$$\hat{H}_{\text{LZSM}}(t) = \frac{\hbar}{2} \left( \delta + \omega_p \frac{v(t)}{c} \right) \hat{\sigma}_{\vec{n}}^{(3)} + \frac{g_{\vec{n}}}{2} \hat{\sigma}_{\vec{n}}^{(1)} \quad (4)$$

where  $\delta = \omega_0 - \omega_p$  is the detuning,  $\omega_0$  is the clock transition frequency of  $^{87}\text{Sr}$ ,  $g_{\vec{n}}$  is an effective coupling strength of the atoms with the CL. Notice that the spatial driving enters as an effective modulation proportional to  $v(t)$  while the external degrees of freedoms of the atoms remain unchanged when ignore the small linear potential term in Eq. 2: the vector  $\vec{n} = (n_z, n_r)$  denotes the quantum numbers of the eigenenergies  $E_{\vec{n}}/\hbar = \nu_z(n_z + 1/2) + \nu_r(n_r + 1)$  of the trapping potential having longitudinal and transverse trap frequencies  $\nu_z = 64.8\text{ kHz}$  and  $\nu_r = 250\text{ Hz}$ , respectively.

*Rabi spectroscopy.* — The measurements of the atomic energies are performed by high-precision clock Rabi spectroscopy that operates at a fractional instability of  $10^{-15}$  [31]. A  $\lambda_p = 698\text{ nm}$  the spectroscopic clock laser is locked to an ultralow-expansion cavity having a linewidth of approximately 1 Hz. A slight misaligning between CL and lattice axis, see Fig. 1a, induces a coupling to the suppressed radial motional modes and a correction arising from the thermal distributions on the coupling strength:  $g_{\vec{n}} = g_0 e^{-(\eta_z^2 + \eta_r^2)/2} L_{n_r}(\eta_r^2) L_{n_z}(\eta_z^2)$ , where  $g_0/\hbar = 3.3\text{ Hz}$ , and  $L_n$  is the  $n$ th order Laguerre polynomial with Lamb-Dick parameters  $\eta_z = \sqrt{\hbar/(2M\nu_z)}/\lambda_p$  and  $\eta_r = \sqrt{\hbar/(2M\nu_r)}/\lambda_p$ . At the end of each spectroscopic probe, the number of atoms in the  $|g\rangle$  and  $|e\rangle$  states are determined by using a cycling transition. This provides the normalized population fraction  $P_e$  of the  $|e\rangle$  state. After many repetitions of the measurements, data are collected while the CL is scanned across the clock transition to eventually construct the Rabi spectrum (Fig. 2). Rabi oscillations as a function of the probe pulse time  $t_p$  are shown in Fig. 3. Both the Rabi spectroscopy and the Rabi oscillations are performed while modulating the system with the Floquet periodic driving. Notice that since the measurement processes last

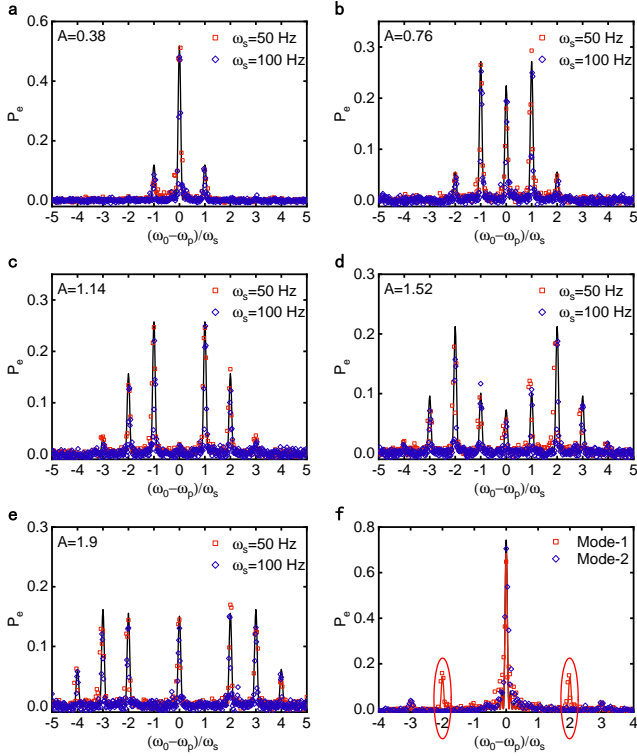


Figure 2. Rabi spectroscopy of the Floquet bands. (a)-(e) Monochromatic driving with different amplitudes  $A$ . The experimental measurements at the probe time  $t_p = 150$  ms and driving frequencies  $\omega_s/2\pi = 50$  Hz (red square) and  $\omega_s/2\pi = 100$  Hz (blue diamond) are compared with theoretical results (solid black line). (f) Three-frequencies driving with two sets of coefficients: Mode-1:  $\vec{A}_1 = \{0.065, 0.345, 0.243\}$  and Mode-2:  $\vec{A}_2 = \{0.005, 0.005, 0.16\}$ . The measured Rabi spectrum of Mode-1 (red square) and Mode-2 (blue diamond) are presented. In both cases, the probe time is  $t_p = 200$  ms and the driving frequency  $\omega_s/2\pi = 50$  Hz. In red ovals, the suppression of the second order FBs when using the Mode-2 set of parameters is shown, demonstrating the possibility of manipulating specific FB. The solid red and black lines are the theoretical Rabi spectrum of Mode-1 and Mode-2, respectively.

only hundreds of milliseconds, we can ignore the spontaneous emission due to the long life time of the excited states. According to the Floquet theory [2], the clock energy levels are split to several Floquet bands (FB) as depicted in Fig. 1c. The experimental results of the Rabi spectroscopy done at different driven modulation amplitudes  $\omega_1$  and frequencies  $\omega_s$  are presented in Fig. 2a-e.

We observe, in particular, that (i) sharp FBs are separated by intervals  $\omega_s$ , each band having a few Hz line-width; (ii) the number of FBs is increasing with the renormalized driven amplitude  $A = \omega_1 \omega_p L / 2 \bar{\omega} L C$ ; (iii) the intensity of Floquet Rabi spectra depends on the values of  $A$  (and not on  $\omega_s$ ) after rescaling the detuning as  $(\omega_0 - \omega_p)/\omega_s$ . These phenomena can be quantitatively understood within the Floquet theory [2]. Because of the ultra-stable narrow optical CL and  $\delta \ll 2\pi\nu_z$ , the Rabi oscilla-

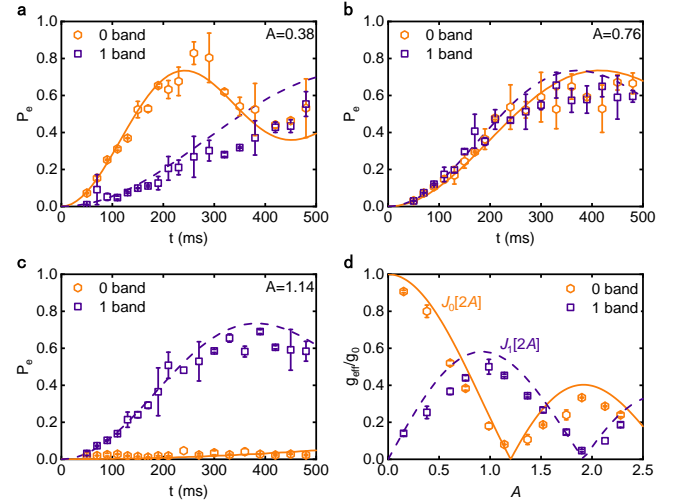


Figure 3. Theoretical (solid lines) and experimental (dashed lines) Rabi oscillations at driven amplitudes (a)  $A = 0.38$ , (b)  $A = 0.76$  and (c)  $A = 1.14$ . The red hexagons are for the zeroth band while the blue squares for first band. (d) The ratio between Floquet modulated Rabi frequencies with Rabi frequencies of the zeroth and first bands measured experimentally are compared with the Bessel function predicted by the Floquet theory.

tions mainly occur within a fixed external quantum numbers  $\vec{n}$ . We can therefore study the dynamical evolution of the spin populations in an extended Hilbert space, consisting of the direct product of the original spin and Floquet quasi-levels  $[|g\rangle, |e\rangle] \otimes [1, e^{\pm i\omega_s t}, e^{\pm 2i\omega_s t}, e^{\pm 3i\omega_s t} \dots]$ . In the resonance region  $\omega_s \gg g_{n_z, n_r}$  [24], we define an effective Rabi frequency for the  $k$ th FB as  $g_{\vec{n}}^k = g_{\vec{n}} J_k[2A]$ , where  $J_k[2A]$  is the  $k$ th order first kind Bessel function. Thus, the excited state population for  $k$ th FB is:

$$P_e^k(\delta, t) = \sum_{\vec{n}} q_z(n_z) q_r(n_r) \left( \frac{g_{\vec{n}}^k}{\hbar R_k} \right)^2 \sin^2 \left[ \frac{R_k}{2} t \right], \quad (5)$$

where  $R_k = \sqrt{(g_{\vec{n}}^k/\hbar)^2 + (\delta - k\omega_s)^2}$ . The  $q_z(n_z)$  and  $q_r(n_r)$  are the statistical distributions of the atoms among the eigen-energies of the lattice trapping potential [32]. It is important to notice here that the atomic statistical distributions in periodically driven systems are, in general, not fully understood in the literature. We could still expect a Boltzmann distribution with an effective temperature since, in our case, the Floquet gap  $\hbar\omega_s/k_B$  ( $k_B$  is the Boltzmann constant) is about a few nK and is much smaller than the longitudinal trap gap energy  $\hbar\nu_z/k_B$  which is several  $\mu$ K. We therefore assume the Boltzmann distributions  $q_{z(r)}(n_{z(r)}) = (1 - Z_{z(r)}) Z_{z(r)}^{n_{z(r)}}$  with  $Z_{z(r)} = e^{-\hbar\nu_{z(r)}/(k_B T_{z(r)})}$  where the longitudinal and transverse trap effective temperatures  $T_z = 2.96 \mu$ K and  $T_r = 3.68 \mu$ K are extracted by the experimental side bands spectra [32].

The quantitative agreement between the theoretical

predictions Eq. 5 and the experimental spectra reported in Fig. 2a-e demonstrates the validity of the Boltzmann statistics assumption. Furthermore, from Eq. 5 we gather that the center of the Rabi spectrum  $P_e^k(\delta, t_p)$  is provided by  $\omega_s$  while the line shapes mainly depends on  $A$ , in agreement with what observed in (i) and (iii). The point (ii) is the direct consequence of the Bessel functions modulations of the Rabi frequency. By increasing the renormalized driven amplitude  $A$ , higher order Bessel functions become relevant and an increasing number of FBs emerges. At the same time, the weights of a few of them may decrease or be totally suppressed, as can be observed in the zeroth band at  $A = 1.14$  and in the first FB at  $A = 1.9$  in Fig. 2. In Fig. 3a-c we show the Rabi oscillations at different values of the strength  $A$ . Notice that at  $A = 1.14$ , the zeroth band is totally eliminated, as also evident from Fig. 2c. We can probe the height  $P_e^k(\delta, t_p)$  of  $k$ th FB at a time  $t_p$  and compare it with the non-driven case at a different time  $t'_p$ , defined as the time when the values of the two peaks are the same. The ratio between Floquet modulated Rabi frequencies and natural Rabi frequency is  $g_{\text{eff}}^k/g_0 = t'_p/t_p = J_k[2A]$ . As shown in Fig. 3d, this Bessel function dependence emerges quite clearly in the experimental results.

We now extend the monochromatic driving to a multi modes periodical function, see Eq.1. In this case the  $k$ th Floquet level is modulated by a rather complex combination of Bessel functions :

$$\mathcal{J}_k[\vec{A}] = \sum_{\{k_1, k_2, \dots, k_N\}} \prod_m J_{k_m}[2A_m] \quad (6)$$

with the constraint  $\sum_m m k_m = k$  and  $A_m \equiv \omega_m \omega_p L / 2 \bar{\omega}_L c$ . By appropriately choosing the values of  $A_m$  of each mode, we independently modulate the FBs while keeping the zeroth band nearly unchanged. As shown in Fig. 2f, the experimental results of three-frequencies driving are in good agreement with the theoretical prediction Eq. 5 after replacing  $J_k[A]$ , with  $\mathcal{J}_k[\vec{A}]$ . It would also be possible to create asymmetric distributions by introducing a phase in each mode.

*Sensitivity of the Rabi spectroscopy.* — At last, we estimate the spectroscopic sensitivity of the modulated optical clock by measuring the Fisher information. The Fisher information (FI) plays a central role in parameter estimation theory, where it determines the Cramer-Rao sensitivity lower bound [21], [25], [26]. The FI is also inversely proportional to the Allan variance [33],  $\sigma_{\text{AI}} \sim 1/(\tau F)$ , where  $\tau$  is the measurement time, whenever time noise correlations of the local oscillator can be neglected. Here the parameter to be estimated is the detuning  $\delta$ , with the Fisher information

$$F(\delta) = \frac{1}{P_e(\delta)(1 - P_e(\delta))} \left( \frac{\partial P_e(\delta)}{\partial \delta} \right)^2. \quad (7)$$

The Eq. 7 is recovered for dichotomic (yes/no) measurement results and therefore coincides with an error

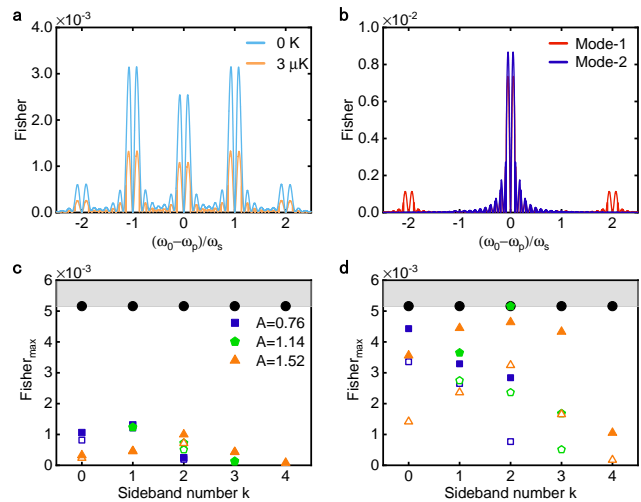


Figure 4. Fisher information of Floquet distributions. (a) The FI as function of rescaling detuning with parameter values as in Fig. 2b. We compare the cases of zero and finite temperatures with  $A=0.76$ ; (b) Comparison of the FI for the Mode-1 and Mode-2 three-frequencies driving case, see Fig. 2f; Experimental (hollow icons) and theoretical (solid icons) values of the maximum Fisher information in case of (c)  $g_0/h = 3.3$  Hz and (d)  $g_0/h = 12$  Hz. The dark filled circles are the maximum theoretical value of the Fisher information, maximized over all possible value of  $g_0$ , at finite temperature. (In these cases, the maximum Fisher information at zero temperature is  $\sim 9.1 \times 10^{-3}$  at  $g_{0m}/h \simeq 3.34$  Hz while the thermal effects reduces it to  $\sim 5.2 \times 10^{-3}$ ).

propagation expression [34]. The higher is the FI, the higher the sensitivity of the estimation. Given the symmetry of the probability distributions, the FI of each band has a two peaks structure, with the maximum determined by the competition between a maximum slope and a minimum fluctuation (provided by the denominator of Eq. 7). In Fig. 4a-b we show the theoretical calculation of the Fisher information at a fixed  $g_0$ . In Fig. 4a we compare the FI at zero and finite temperature. It is evident that the value of FI strongly depends on the Floquet band and is depleted by the temperature of the atomic gas. In Fig. 4b we compare the FI for the Mode-1 and Mode-2 three-frequencies drive. In Fig. 4c-d we compare the theoretical values of the FI obtained with  $P_e(\delta, t)$  given by Eq. 5, with the experimental results obtained from the Rabi spectra reported in Fig. 2. The black filled circles report the theoretical value of the FI maximized over all possible values of  $g_0$ . The theoretical values agree with the experimental results within a factor 2, in average. This is remarkable given that the theoretical Fisher information has been calculated by only taking in account temperature effects but not other source of decoherence like the laser fluctuations that are present in the experimental realizations.

*Conclusion and outlook.* — We have engineered an optical atomic clock by periodically driving the trap-

ping lattice potential. We have resolved with Rabi spectroscopy several Floquet quasi-energy bands. We have demonstrated the possibility to selectively manipulate a chosen band by appropriately adjusting the driven amplitudes of different driving modes. In future work, it will be possible to shape the inter-well tunneling barriers of the lattice by modulating the potential of Eq. 2 as already demonstrated in [6–14]. The spin-lattice coupling Hamiltonian Eq. 3 can be switched on to introduce entanglement between spatial and spin coordinates. Furthermore, it will be possible to control the inter-atomic interaction in bosonic clocks with Feshbach resonances [35]. These explorations will open to the possibility of creating a novel generation of quantum simulators with the experimental measure of the Fisher information witnessing multiparticle entanglement [36, 37].

*Acknowledgment.* — Discussions with A. Bertoldi, L. Pezzé and N. Poli are acknowledged. This work is supported by the National Science Foundation of China (Grant No. 61775220), the Key Research Project of Frontier Science of the Chinese Academy of Sciences (Grant No. QYZDB-SSW-JSC004) and the Strategic Priority Research Program of the Chinese Academy of Sciences (Grant No. XDB21030100). T. W. is supported by the Special Foundation for theoretical physics Research Program of China (No. 11647165). X.-F. Z. acknowledges funding from the National Science Foundation of China (Grants No. 11804034, No. 11874094 and No. 11947406) and Chongqing Natural Science Foundation (Grant No. cstc2018jcyjAX0399). W.-D. L. and A. S. acknowledge the fundings from the National Science Foundation of China (No. 11874247 and No. 11874246), the National Key R&D Program of China (Grant No. 2017YFA0304501), 111 project (Grant No. D18001), the Hundred Talent Program of the Shanxi Province (2018). A. S. acknowledges funding of the project EMPIR-USOQS, EMPIR projects are co-funded by the European Unions Horizon2020 research and innovation programme and the EMPIR Participating States.

---

\* These authors contributed equally to this work.

† zhangxf@cqu.edu.cn

‡ wdli@sxu.edu.cn

§ augusto.smerzi@ino.it

¶ changhong@ntsc.ac.cn

- [1] M. S. Rudner and N. H. Lindner, *Nat. Rev. Phys.* **2**, 229 (2020).
- [2] A. Eckardt, *Rev. Mod. Phys.* **89**, 011004 (2017).
- [3] M. Bukov, L. D’Alessio, and A. Polkovnikov, *Adv. Phys.* **64**, 139 (2015).
- [4] M. C. Rechtsman, J. M. Zeuner, Y. Plotnik, Y. Lumer, D. Podolsky, F. Dreisow, S. Nolte, M. Segev, and A. Szameit, *Nature* **496**, 196 (2013).
- [5] P. Roushan, C. Neill, A. Megrant, Y. Chen, R. Babush, R. Barends, B. Campbell, Z. Chen, B. Chiaro, A. Dunsworth, A. Fowler, E. Jeffrey, J. Kelly, E. Lucero, J. Mutus, P. J. J. O’Malley, M. Neeley, C. Quintana, D. Sank, A. Vainsencher, J. Wenner, T. White, E. Kapit, H. Neven, and J. Martinis, *Nat. Phys.* **13**, 146 (2017).
- [6] H. Lignier, C. Sias, D. Ciampini, Y. Singh, A. Zenesini, O. Morsch, and E. Arimondo, *Phys. Rev. Lett.* **99**, 220403 (2007).
- [7] A. Zenesini, H. Lignier, D. Ciampini, O. Morsch, and E. Arimondo, *Phys. Rev. Lett.* **102**, 100403(2009).
- [8] J. Struck, C. Ischlger, R. Le Targat, P. Soltan-Panahi, A. Eckardt, M. Lewenstein, P. Windpassinger, and K. Sengstock, *Science* **333**, 996(2011).
- [9] F. Grg, M. Messer, K. Sandholzer, G. Jotzu, R. Desbuquois, and T. Esslinger, *Nature* **553**, 481(2018).
- [10] J. Struck, M. Weinberg, C. Ischlger, P. Windpassinger, J. Simonet, K. Sengstock, R. Hppner, P. Hauke, A. Eckardt, M. Lewenstein, and L. Mathey, *Nat. Phys.* **9**, 738(2013).
- [11] N. R. Cooper, J. Dalibard, and I. B. Spielman, *Rev. Mod. Phys.* **91**, 015005 (2019).
- [12] M. Aidelsburger, M. Atala, M. Lohse, J. T. Barreiro, B. Paredes, and I. Bloch, *Phys. Rev. Lett.* **111**, 185301(2013).
- [13] H. Miyake, G. A. Siviloglou, C. J. Kennedy, W. C. Burton, and W. Ketterle, *Phys. Rev. Lett.* **111**, 185302(2013).
- [14] G. Jotzu, M. Messer, R. Desbuquois, M. Lebrat, T. Uehlinger, D. Greif, and T. Esslinger, *Nature* **515**, 237(2014).
- [15] S. Kolkowitz, I. Pikovski, N. Langellier, M. D. Lukin, R. L. Walsworth, and J. Ye, *Phys. Rev. D* **94**, 124043(2016).
- [16] M. A. Norcia, J. R. K. Cline, and J. K. Thompson, *Phys. Rev. A* **96**, 042118(2017).
- [17] H. Katori, M. Takamoto, V. G. Pal’chikov, and V. D. Ovsiannikov, *Phys. Rev. Lett.* **91**, 173005(2003).
- [18] J. I. Cirac and P. Zoller, *Nat. Phys.* **8**, 264(2012).
- [19] I. Bloch, J. Dalibard, and S. Nascimbène, *Nat. Phys.* **8**, 267(2012).
- [20] C. Gross and I. Bloch, *Science* **357**, 995(2017).
- [21] L. Pezzè, A. Smerzi, M. K. Oberthaler, R. Schmied, and P. Treutlein, *Rev. Mod. Phys.* **90**, 035005(2018).
- [22] W. F. McGrew, X. Zhang, R. J. Fasano, S. A. Schffer, K. Beloy, D. Nicolodi, R. C. Brown, N. Hinkley, G. Milani, M. Schioppo, T. H. Yoon, and A. D. Ludlow, *Nature* **564**, 87(2018).
- [23] M. Sillanp, T. Lehtinen, A. Paila, Y. Makhlin, and P. Hakonen, *Phys. Rev. Lett.* **96**, 187002(2006).
- [24] S. N. Shevchenko, S. Ashhab, and F. Nori, *Phys. Rep.* **492**, 1(2010).
- [25] L. Pezzè and A. Smerzi, *Quantum theory of phase estimation*, *Atom Interferometry, Proceedings of the International School of Physics “Enrico Fermi”, Course 188*, edited by G. M. Tino and M. A. Kasevich, Varenna, (IOS Press, Amsterdam, 2014), p. 691–741.
- [26] V. Giovannetti, S. Lloyd, and L. Maccone, *Nat. Photonics* **5**, 222(2011).
- [27] M. Takamoto and H. Katori, *Phys. Rev. Lett.* **91**, 223001(2003).
- [28] M. Takamoto, F.-L. Hong, R. Higashi, and H. Katori, *Nature* **435**, 321(2005).
- [29] O. Mandel, M. Greiner, A. Widera, T. Rom, T. W. Hansch, and I. Bloch, *Phys. Rev. Lett.* **91**, 010407(2003).
- [30] H.-N. Dai, B. Yang, A. Reingruber, X.-F. Xu, X. Jiang, Y.-A. Chen, Z.-S. Yuan, J.-W. Pan, *Nat. Phys.* **12**, 783(2016).

- [31] Y.-B. Wang, X.-T. Lu, B.-Q. Lu, D.-H. Kong, and H. Chang, *Appl. Sci.* **8**, 2194(2018).
- [32] S. Blatt, J. W. Thomsen, G. K. Campbell, A. D. Ludlow, M. D. Swallows, M. J. Martin, M. M. Boyd, and J. Ye, *Phys. Rev. A* **80**, 052703(2009).
- [33] F. Rihle, *Frequency Standards: Basics and Applications* (Wiley-VCH, Berlin, 2004), Chap.3, p. 60.
- [34] W. M. Itano, J. C. Bergquist, J. J. Bollinger, J. M. Gilligan, D. J. Heinzen, F. L. Moore, M. G. Raizen, and D. J. Wineland, *Phys. Rev. A* **47**, 3554(1993).
- [35] C. Chin, R. Grimm, P. Julienne, and E. Tiesinga, *Rev. Mod. Phys.* **82**, 1225(2010).
- [36] L. Pezzè and A. Smerzi, *Entanglement*, *Phys. Rev. Lett.* **102**, 100401(2009).
- [37] L. Pezzè, Y. Li, W.-D. Li and A. Smerzi, *Witnessing entanglement without entanglement witness operators*, *PNAS* **113**, 11459(2016).